A Far-Field Matching Method for Transonic Computations

Allen W. Chen*
Boeing Commercial Airplane Company, Seattle, Wash.
and
Lawrence J. Dickson† and Paul E. Rubbert‡
Boeing Aerospace Company, Seattle, Wash.

In solving a mixed-type (elliptic-hyperbolic) differential equation in an unbounded region, which is elliptic near infinity, some way must be found to transfer the boundary conditions at infinity to a finite artificial boundary in order to keep the discretized problem finite. The common example of this is transonic flow over an airfoil or wing with subsonic freestream. Here we present an approach which is in many ways analogous to the "adaptive wind-tunnel wall" concept. Iterative revision of a Dirichlet condition on the common or "matching" boundary of the near and far fields results in convergence to a far-field solution that matches the discretized near-field solution in potential and normal derivative across the matching boundary. The far-field equation is either a first-order (FO) Prandtl-Glauert, or a second-order (SO) Poisson-type approximation to the transonic equation. A parameter is easily calculated which gives a good estimate of the accuracy of the far-field solution in either case. Two-dimensional results are given showing the success of the method in reproducing the circulation and C_p for a lifting airfoil. Accurate solutions are given using far-field matching boundaries which are much closer to the airfoil than is permissible with Klunker-type far fields based on multipole expansions. The results are shown to be invariant with the location of the vortex representing the far-field circulation. Thus, we significantly reduce computer time by factors of 3 (FO) and 7 (SO) for mesh density and accuracy equivalent to those of a fixed asymptotic far-field representation. Nonlifting FO calculations for a three-dimensional rectangular wing similarly yield accurate results for a much reduced near field, cutting computer time by more than a factor of 2 in an unoptimized case where the minimum boundary size has not yet been established.

I. Introduction

THE imposition of the outer boundary conditions on the discretized transonic problem typically has been carried out either by transformations mapping the infinite region to a finite one, with infinity mapped to a singular point, or by asymptotic far-field expansions. The first approach has been used by Bauer et al.[1] Jameson,[2] and others in two dimensions, but is not suitable for three-dimensions. The second approach, with the Prandtl-Glauert asymptotic expansion carried out to one or two terms – a lifting vortex and a doublet distribution depending on a thickness integral – has been used by Krupp and Murman[3] and Klunker[4] in two-dimensions, and Bailey and Ballhaus[5] and Schmidt[6] in three-dimensions. Schmidt matches normal derivative across the matching boundary; the others match the potential. Since it is not possible to match both, and since the assumptions behind the asymptotic expansion doublet coefficient treat the flow (erroneously) as a subsonic perturbation flow in the inner field, serious errors may be introduced by this matching.

The present approach,[7] in the first-order (FO) case, expressed the far-field flow as a linear combination of a Prandtl-Glauert vortex, centered somewhere in the near field, and source distributions (whose construction is described in Appendix A) along the matching boundary. The second-order (SO) solution is constructed similarly, with quadratic Poisson correction terms added. The matching boundary condition is determined iteratively by a method described and justified in Appendix B. Briefly, a Dirichlet condition on the matching boundary, which is imposed on both the near-field and far-field solutions, is periodically adjusted to reduce to zero the normal derivative discontinuity across the matching boundary.

The present method has the two advantages of being self-correcting and of operating with many more degrees of freedom than the asymptotic methods. This makes it insensitive to changes in the location of the matching boundary and/or the lifting vortex distribution. The only errors, other than discretization errors, in a converged and matched solution are those resulting from the deviation of the FO or SO far-field equation from the nonlinear equation. These are easily estimated[7] and are confirmed by computational experiment. This confidence in the boundary conditions enables the user with limited computer capacity to do one or more of the following: reduce computer time, increase near-field mesh density, or optimize the iterative circulation boundary condition.

II. Theory

We merely summarize the theory here; more detail is found in Appendices A and B, and in Ref. 7. We use the Guderley-von Karman transonic small perturbation equation, which in three-dimensional flux formulation is

$$\left(K\phi_x - K_\gamma \frac{\phi_x^2}{2}\right)_x + (\phi_y)_y + (\phi_z)_z = 0$$

Here $K = \beta^2 = 1 - M_\infty^2$, while $K_\gamma = M_\infty^2(\gamma+1)$, $\gamma = 1.4$ for air, $M_\infty < 1$ (subsonic freestream). First-order far-field solutions are chosen from a linear set of solutions to the Prandtl-Glauert equation

$$K\phi_{xx}^{(1)} + \phi_{yy}^{(1)} + \phi_{zz}^{(1)} = 0$$

Second-order solutions are of the form $\phi^{(2)} = \phi^{(1)} + \psi$, where $\phi^{(1)}$ is of the preceding form, and ψ is a small correction term satisfying

Presented as Paper 77-208 at the AIAA 15th Aerospace Sciences Meeting, Los Angeles Calif., Jan. 24-26, 1977; submitted March 9, 1977; revision received July 5, 1977.

Index categories: Aerodynamics; Subsonic Flow; Transonic Flow.

*Specialist Engineer, Aerodynamic Research Unit. Member AIAA.

†Senior Engineer, Aerodynamic Research Unit.

‡Supervisor, Analysis Methods Group, Aerodynamic Research Unit. Associate Fellow AIAA.

$$K\psi_{xx}+\psi_{yy}+\psi_{zz}=K_\gamma\frac{\partial}{\partial x}\left[\frac{(\phi_x^{(I)})^2}{2}\right]$$

The two-dimensional expressions follow from the foregoing by eliminating spanwise derivatives.

As explained in Ref. 7, the key parameter used in predicting the applicability of the expansions is

$$\epsilon=\max_{[\text{far field}]}|\phi_x|/\phi_{x_{\text{sonic}}}$$

where $\phi_{x\,\text{sonic}}=K/K_\gamma$. Then we require $\epsilon<1$, and estimate the error caused by the far-field approximations as $O(\epsilon^2)$ in the FO case, and $O(\epsilon^3)$ in the SO case. This is borne out by computational experiment. The SO method fails to converge for ϵ greater than about 0.5; this has been found to be due to discretization errors in the sensitive SO correction terms, which destroy the elliptic character of the discretized problem.

The solution procedure starts from the finite-difference near field and an outer field solution produced by a panel method, both subject to the same Dirichlet boundary condition along the matching boundary. After a number of sweeps, the far field is updated by adding the influence of a source sheet distributed along the matching boundary of strength equal, in one method, to that required to cancel the discontinuity in normal velocity across the matching boundary that evolves after the first iteration sweeps. This produces a new value of the velocity potential along the matching boundary on the side facing the far field. This potential distribution is then applied as an updated Dirichlet condition for the near field, which is then swept using this Dirichlet condition, typically about 50 times.

This first-order update sequence is repeated until convergence (achieved when ϕ and $\partial\phi/\partial n$ are both continuous across the matching boundary) or a second-order update. The second-order update changes the linearized aerodynamic influence coefficients (AIC's) of the elementary far-field distributions. The near field is then swept and first-order updates repeated as before.

For lifting flows, the circulation is updated after every sweep. Strong under-relaxation (factor near 0.2) is used where the full value of the circulation change is what would be required to satisfy the Kutta condition if the perturbation flow were Prandtl-Glauert about a flat plate. At this time, second-order far-field and lifting cases have been fully developed only for two-dimensional flows.

III. Results

Two-Dimensional Flows

The two-dimensional results presented here are for a nonsymmetric, lifting airfoil that is flat on the bottom and parabolic on top, with maximum thickness 6% of chord (Fig. 1). Airfoil boundary conditions are linearized on the slit $0\le x\le 1$, $y=0$. There are 16 equally spaced finite-difference (FD) meshes over the airfoil in the x direction, and the mesh height starts at 0.025 chord, with the mesh dimensions stretching with a mesh ratio of 1.2 away from the airfoil in both the x and y directions. The differencing method is a modification of the first-order conservative Murman-Cole approach that admits arbitrary mesh variation away from the supersonic region.[8] The solutions were converged until the residual (flux generation per unit area) was less than 0.0001 in the worst cell, and, where applicable, the last first-order and last second-order corrections each introduced an additional residual error <0.0001. The two-dimensional results in the figures are all for $M_\infty=0.77$ and $\alpha=0$ deg.

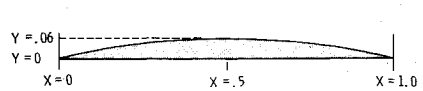

Fig. 1 Asymmetric airfoil shape for two-dimensional sample cases.

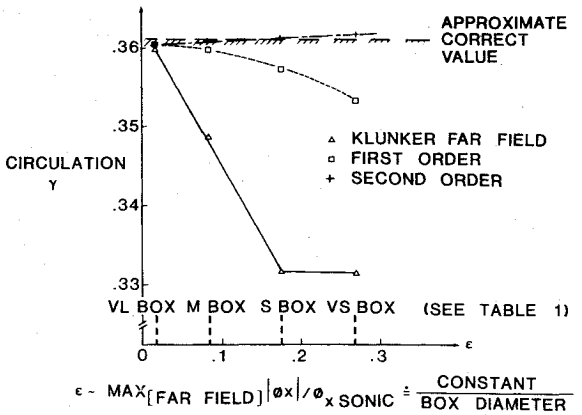

Fig. 2 Circulation as function of box size.

Two methods were used for the two-dimensional FO updates. The "new" method, described and justified in Appendix B, is to update the far field by revising the source strength along the matching boundary by an amount such that, if the resulting linearized correction were extended over *both* the outer and inner field, the normal velocity jump would be eliminated. This method, which is computationally less expensive (no AIC matrix solving) and theoretically more general, results in a slight improvement over the rate of convergence of the older method, used in Ref. 7. The method used in Ref. 7 is to adjust the far field by a far-field equation solution which has, as Neumann condition along the matching boundary, half the normal velocity jump there. For consistency's sake, it is used in the two-dimensional results shown here in the figures.

Figure 2 shows the converged value of the circulation for various far-field boundary box sizes listed in Table 1. This sensitive scalar gives a good indication of the quality of the outer boundary conditions. As expected, the error caused by the SO far field is $O(\epsilon^3)$, and that associated with FO far field is $O(\epsilon^2)$. For each box, the vortex and (for Klunker's results) the doublet were at $(0.5c,0)$. In the case of the very small (VS) box, the vortex is rather near the lower boundary, and a peculiarity in the Klunker result (see Fig. 4) caused by the resulting tendency toward stagnation in the lower far field. The boundary sources in the matching methods did a good job of cancelling this effect.

Figure 3 plots accuracy of circulation over computation sweeps and computer times. To avoid repeating a costly calculation, the FO and SO results for the VL box were calculated using the Klunker result as a starting point, and the cost figures shown in these cases are the Klunker figures plus the subsequent FO or SO costs. Here, it was found necessary to impose the condition $\int_B\phi=0$, where B is the matching boundary, on all first-order iterations to get convergence; it also speeds convergence for the smaller boxes. For those boxes, all runs were initialized by setting $\phi=0$.

The Kutta condition in each case is to require smoothness of ϕ_x in the y direction at the trailing edge; the four nearest values – two above and two below the trailing edge – are required to lie on a parabola. The circulation is adjusted each sweep, along with the potential jump at the wake, by a

Table 1 Location of matching boundaries, and values of ϵ, for $M_\infty=0.77$, $\alpha=0$ deg, $\epsilon=\max_{[\text{far field}]}|\phi_x|/\phi_{x\,\text{sonic}}$

Box	$X_{\min}/C$	$X_{\max}/C$	$Y_{\min}/C$	$Y_{\max}/C$	ϵ
1. Very large (VL)	−11.762	12.762	−19.65	19.65	0.0165
2. Medium (M)	− 1.394	2.394	− 3.627	4.397	0.083
3. Small (S)	− 0.429	1.429	− 1.065	2.45	0.175
4. Very small (VS)	− 0.15625	1.15525	− 0.521	1.633	0.27
5.	− 0.09375	1.09375	− 0.135	0.85	0.6

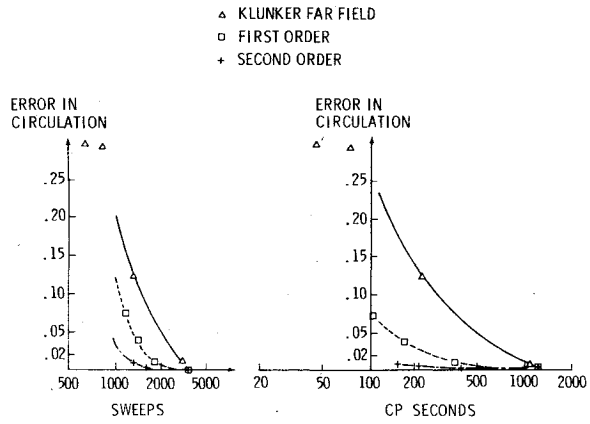

Fig. 3 Error as function of effort.

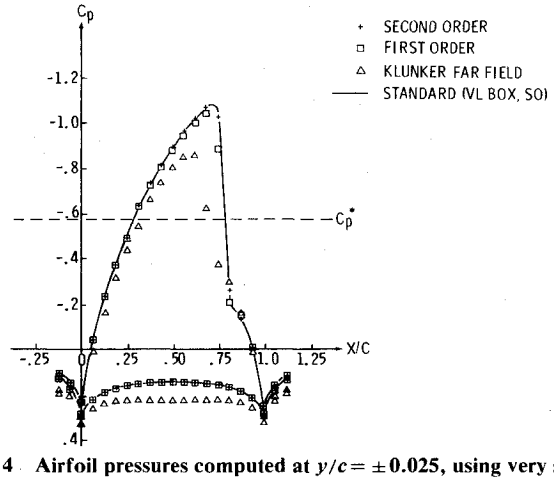

Fig. 4 Airfoil pressures computed at $y/c = \pm 0.025$, using very small box.

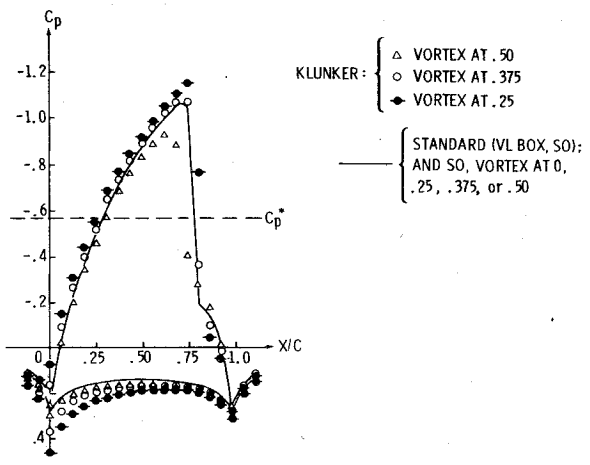

Fig. 5 Small box: dependence of Klunker C_p on vortex location.

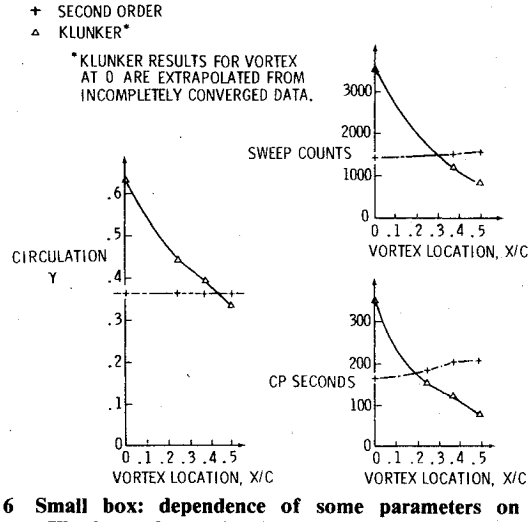

Fig. 6 Small box: dependence of some parameters on vortex location—Klunker and second order.

fraction of that amount which would correct for the deviation from the Kutta condition if the airfoil were a flat plate and the flow equation were Prandtl-Glauert. By keeping the under-relaxation factor small (near 0.2), we avoided any instabilities. This contrasts with Krupp[9] and Schmidt,[6] where less frequent circulation updates were needed for stability.

Figure 4 shows airfoil C_p plots for the VS box. The standard case (VL box, SO) is assumed to be to within the convergence tolerance, equal to the solution with the matching boundary at infinity (see Fig. 2). Notice the "dip" in the lower surface Klunker C_p. This is due to the relative closeness of the vortex to the lower matching boundary.

Figure 5 illustrates the strong dependence of the Klunker solution on the vortex location (the thickness doublet was at the centroid of the airfoil thickness distribution). The FO and SO solutions did not change perceptibly when the vortex was moved. Circulation values, convergence times, and sweep counts for various vortex locations are shown in Fig. 6. By moving the vortex in the y direction so that it was centered between the top and bottom of the box, FO and SO convergence were further speeded.

These solutions' independence of their convergence history, also evident when we compared the results of the "old" and "new" FO updating methods, is of interest as evidence that the conservative Murman-Cole discretization of the transonic equations actually does give a unique solution.

The method has been tested for a variety of freestream Mach numbers up to 0.85 for the M box. A supersonic-to-supersonic trailing edge shock, with another shock aft of the trailing edge, was found at $M_\infty = 0.85$, $\alpha = 6$ deg. The matching method or Kutta condition never generated any instabilities, given suitable under-relaxation (0.6 to 1.0 for the matching and about 0.2 for the Kutta), except that the SO method diverged for box No. 5 (see Table 1). This divergence has been experienced before for $\epsilon > 0.5$, and is due to discretization errors destroying the elliptic character of the discrete far-field equation at the matching boundary, as we found by examining the AIC matrix.

Three-Dimensional Flows

The configuration analyzed is a rectangular wing of $AR = 6$ with constant NACA 0012 sections. Freestream Mach number is 0.82 and the angle of attack is 0 deg. Computations were made using a large box ($-15 \le x/c \le 16$, $|\eta| = |2y/b| \le 4.9$, $|z/c| \le 18$) and a small box ($-0.62 \le x/c \le 1.55$, $|\eta| \le 1.2$, $|z/c| \le 1.88$). In addition to applying the far-field matching technique described in Sec. II, computations also were made using three other types of boundary conditions: 1) $\phi = 0$, 2) Klunker's expression, and 3) modified Klunker expression. The modified Klunker expression was obtained by following Klunker's derivation[4] with two exceptions. One is that the spanwise integration was carried out, taking advantage of the rectangular planform and the constant wing sections. The other is to place the resulting doublet at the centroid of the thickness distribution rather than $x = 0$, $y = 0$, $z = 0$, which is the leading edge of the root section. The results are shown in Fig. 7. The large-box solutions obtained from different far-field boundary conditions are indistinguishable from each other and can be considered to be identical for all practical purposes. The small box with $\phi = 0$ did not generate good results, as expected. The small box with Klunker's expression[4] generated stronger expansions and shocks at the

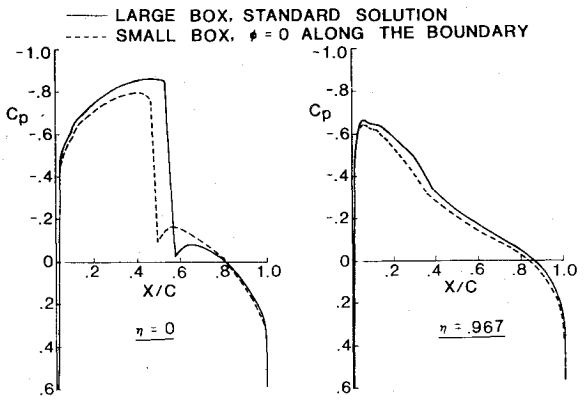

a) Small box results using $\phi = 0$ for far-field boundary condition.

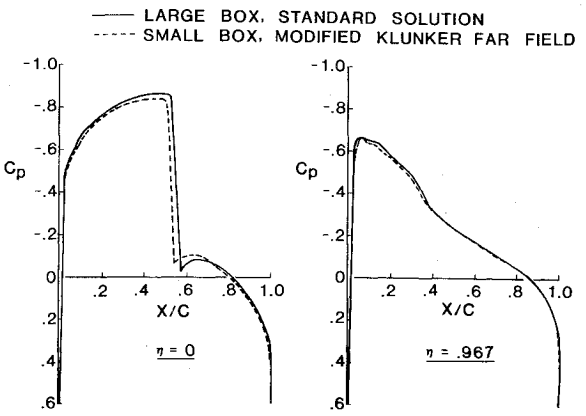

c) Modified Klunker far-field results.

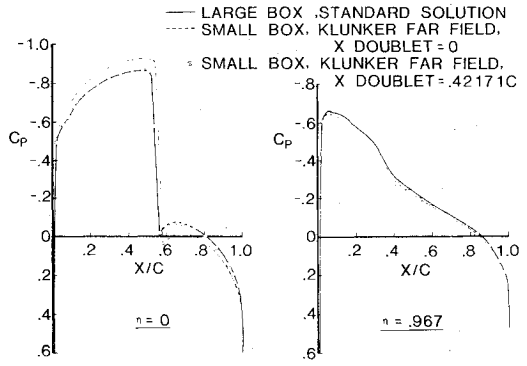

b) Sensitivity of Klunker far-field to thickness doublet location.

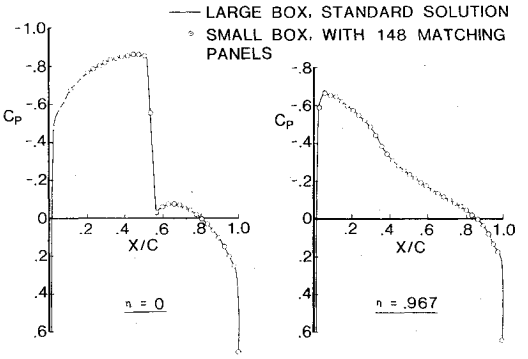

d) Results using far-field matching.

Fig. 7 Pressure distributions on a rectangular wing.

wing root than the standard solution. This is because the upstream boundary is so close to the wing that the error due to placing the doublet at $x=0$, $y=0$, $z=0$ begins to appear. Moving the doublet to the centroid of the thickness distribution improved the results at the wing root, but significant errors remained at the wing tip. The modified Klunker's expression produced results fairly close to the standard solution, but with noticeable discrepancies. The FO method with 148 matching panels reproduced the standard solution for all spanwise stations, $\epsilon = 0.126$ for this sample case. The computation time was reduced from that of the large box by over 50% (see Table 2). An even greater time saving can be expected when the second-order far field is used and the box size is reduced.

The additional computer storage needed for the matching panel influence coefficient matrices is much less than the savings resulted from not having to use finite-difference mesh points for the large flow domain. The net result is a reduction of the total computer storage needed for solving the problem.

IV. Conclusion

The method of matching two flowfield solutions across an artificial boundary has been applied to two-dimensional lifting and three-dimensional nonlifting transonic flows. In the two-dimensional case, both a first-order and a second-order approximation to the transonic equation in the far field are tried; in the three-dimensional case, only the first-order method is used. Results are compared with those of a Klunker asymptotic expansion of the usual type in the far field, using lift and thickness terms.

The results demonstrate the following advantages of the matching method over the asymptotic expansion:

1) Computing cost can be reduced, or, alternately, mesh density increased while holding computing cost constant, by using a smaller near field.

2) Less attention need be given to the form or location of the expression representing the far-field circulation; the result is essentially independent of this.

3) Accuracy can easily be estimated as $O(\epsilon^2)$ for first order, and $O(\epsilon^3)$ for second-order methods, where ϵ is defined as stated earlier.

Table 2 Computing cost for three-dimensional flows

	Total number of finite difference sweeps	Total CP, sec	Far-field updates
Large box with $\phi=0$ along the boundary	266	1821	0
Small box with matching panels	269	829	20

Appendix A: Modeling of Far-Field Flow

In two-dimensions, the FO far-field solution is expressed as a linear combination of elementary Prandtl-Glauert source distributions on the matching boundary and (for lifting flows) a vortex centered somewhere in the near field. In the present work, the matching boundary is a convex polygon. If one assumes (see Appendix B) that the far-field solution at each stage can be extended across the matching boundary, it follows that it has a gradient at each corner, and this gradient is wholly determined by the function values on the sides meeting the corner. Since the corner is convex, the inner solution has the same gradient, and the normal velocity jump goes to zero at the corner.

Thus, we are justified in discretizing the source strength distribution $\sigma(\xi)$, ξ an arc length variable along the matching boundary, by linear combinations of elementary distributions $\sigma_j(\xi)$ as in Fig. 8. Here $\{\xi_j\}$ is an ordered set of nodes chosen on the matching boundary and including the four corners. But if ξ_{j0} is a corner, σ_{j0} is not included in the set of elementary

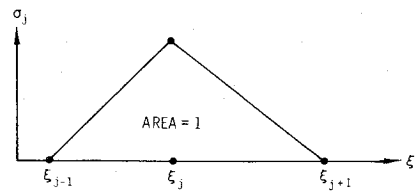

Fig. 8 Elementary singularity strength distribution for two-dimensional linear varying sources on matching boundary.

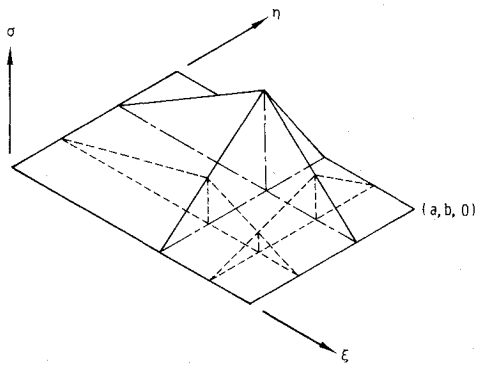

Fig. 9 Elementary singularity strength distribution for three-dimensional bilinear varying sources on matching boundary.

distributions. Thus, this set spans the space of source distributions that are piecewise linear in ξ, with ξ_j as nodes, and zero at the corners.

For each of the σ_j in the basis, $[x_0(\xi), y_0(\xi)]$ is linear for $\xi_{j-1} \le \xi \le \xi_{j+1}$. A Prandtl-Glauert point source induces velocity potential given by $(1/2\pi\beta)\ \ell n\ r$, where $r^2 = x^2 + \beta^2 y^2$. Here $x = \bar{x} - x_0(\xi)$, $y = \bar{y} - y_0(\xi)$, where $(\bar{x}, \bar{y})$ is a control point and (x_0, y_0) is the location of the source. It is easy, by linearity, to find a function $F(\xi)$ such that $F''(\xi) = f(\xi) = (1/2\pi\beta)\ \ell n\ r$. Then one can take advantage of the general distributional formula

$$\int \sigma_j(\xi) F''(\xi)\ d\xi = \int F(\xi)\ d\sigma_j'(\xi) = (\Delta_\xi^2)_j F$$

where $(\Delta_\xi^2)_j$ is the second difference operator evaluated at $\xi_{j-1}, \xi_j, \xi_{j+1}$. Thus,

$$\frac{1}{2\pi\beta} \int \sigma_j(\xi)\, \ell n\ r\ d\xi = 2\left[\frac{F(\xi_{j-1})}{(\xi_j - \xi_{j-1})(\xi_{j+1} - \xi_{j-1})} + \frac{F(\xi_j)}{(\xi_{j-1} - \xi_j)(\xi_{j+1} - \xi_j)} + \frac{F(\xi_{j+1})}{(\xi_{j-1} - \xi_{j+1})(\xi_j - \xi_{j+1})} \right]$$

The second-order source terms are similar, except that they are corrected to give a linearized approximation to the solution of the Poisson equation described in Sec. II.

The three-dimensional FO case proceeds analogously. The assumption that the matching boundary is a convex polygon allows one to conclude, as in the preceding, that the normal derivative discontinuity goes to 0 at edges and corners. If the sides of the polygon are rectangles, as they are in our work, one can model the source distribution on a side by taking linear combinations of elementary bilinear source distributions (Fig. 9). Here ξ and η are linear variables running parallel to the edges, and $x_0(\xi, \eta)$, etc. are linear. As in the foregoing, we find that

$$\int\int \sigma(\xi, \eta) F_{\xi\xi\eta\eta}(\xi, \eta)\ d\xi\ d\eta = \Delta_\xi^2 \Delta_\eta^2 F$$

where Δ_ξ^2 and Δ_η^2 are the respective second-order difference operators in these variable, evaluated at the points $\{\xi_i, i = 1,2,3\}$ and $\{\eta_j, j = 1,2,3\}$ where σ has nodes $\{(\xi_i, \eta_j)\}$.

To evaluate F, one may use the fact that $F_{\xi\xi\eta\eta} = f$ if and only if

$$F = \xi\eta \int_\xi \int_\eta f - \xi \int_\xi \int_\eta \eta f - \eta \int_\xi \int_\eta \xi f + \int_\xi \int_\eta \xi\eta f$$

If one transforms linearly so f satisfies Laplace's equation, $f = -(1/r)$ where $r^2 = (\bar{x} - \xi)^2 + (\bar{y} - \eta)^2 + (\bar{z} - \zeta)^2$, one then finds, after setting $x = \bar{x} - \xi$ etc.,

$$F = -\frac{1}{3} r^3 + \frac{r}{2}(x^2 + y^2) - \frac{x}{2}(y^2 - z^2) \tanh^{-1}\left(\frac{x}{r}\right) - \frac{y}{2}(x^2 - z^2) \tanh^{-1}\left(\frac{y}{r}\right) + xyz \tan^{-1}\left(\frac{xy}{zr}\right)$$

For the three-dimensional flows, the aerodynamics influence coefficients (AIC) for the induced velocity also are needed and they are obtained from

$$F_x = \int_\xi \int_\eta \int_\eta f = \eta \int_\xi \int_\eta f - \int_\xi \int_\eta \eta f$$

$$= -y\left[x \tanh^{-1}\left(\frac{y}{r}\right) + y \tanh^{-1}\left(\frac{x}{r}\right) - z \tan^{-1}\left(\frac{xy}{zr}\right)\right] + \frac{xr}{2} + \frac{y^2 + z^2}{2} \tanh^{-1}\left(\frac{x}{r}\right)$$

$$F_y = \int_\xi \int_\xi \int_\eta f = \xi \int_\xi \int_\eta f - \int_\xi \int_\eta \xi f$$

$$= -x\left[x \tanh^{-1}\left(\frac{y}{r}\right) + y \tanh^{-1}\left(\frac{x}{r}\right) - z \tan^{-1}\left(\frac{xy}{zr}\right)\right] + \frac{yr}{2} + \frac{x^2 + z^2}{2} \tanh^{-1}\left(\frac{y}{r}\right)$$

$$F_z = \int_\xi \int_\xi \int_\eta \int_\eta \frac{\partial}{\partial z}\left(-\frac{1}{r}\right) = xy \tan^{-1}\left(\frac{xy}{zr}\right) + xz \tanh^{-1}\left(\frac{x}{r}\right) + yz \tanh^{-1}\left(\frac{y}{r}\right) - zr$$

For flowfields involving lift, an internal doublet panel with variable strength in the spanwise direction is needed to provide the proper potential jump across the wake at the downstream boundary. The development of the second-order approximation is not completed at this time.

Appendix B: Proof of Convergence of the Matching Method

The matching method mentioned in the Introduction, the "new" matching method of Sec. III, is an iterative procedure. The flowfield of interest is divided into an inner and outer field by a "matching boundary"; it is assumed that the differential equation to be solved is elliptic in the outer field and at the matching boundary. One starts with an outer field solution that can be extended across the matching boundary (commonly either 0, or the result of the previous iteration). There are two steps in each iteration: 1) the differential equation is solved in the inner field, satisfying the Dirichlet condition of being continuous with the outer field solution at the matching boundary and 2) a linearized source, or Green's function, distribution along the matching boundary is generated that, when added to the solution of 1, cancels the normal velocity discontinuity (which is assumed small). Some condition, such as zero integral along the matching boundary, is imposed to enforce uniqueness of this distribution. The sum imposes a new Dirichlet condition, which is satisfied by a solution approximately equal to the extendible linearized solution. One can thus return to step 1.

Two approximations are employed to make the method useful. The equation in the outer field is replaced by a linear or second-order approximation, for which solutions and Green's function distributions can easily be expressed. Also, the inner field solution is incompletely converged between updates, so that the inner field solution and the matching method reach convergence together, thus saving computer time.

Let the outer field be denoted by E, inner field by C, the matching boundary by B, and the airfoil surface by A. It is shown later for Laplace's equation that the matching method always leads to convergence to the correct solution on $E \cup C$ for a Neumann condition on A, when started from $\phi = 0$ in E, if the solution ϕ is continuous on A. The Neumann solution that is found is the one which has zero derivative at ∞ and satisfies $\int_B \phi = 0$ (the last condition merely fixes a constant of integration).

Since the equation is linear, we may subtract the final solution and replace our Neumann condition on A with 0, while starting with a nonzero outer initial function ϕ_0 which can be extended harmonically to A and there satisfies Neumann condition N_0 (the negative of our original Neumann condition). We need only prove that ϕ_j, the outer function after the jth iteration, converges to 0. In fact, we shall prove that it, too, can be extended to A, and there satisfies a Neumann condition N_j such that

$$\int_A |N_j| \le c \int_A |N_{j-1}| \le c^j \int_A |N_0|, \qquad j \ge 1 \tag{B1}$$

for a constant $c < 1$ independent of j. Since the far-field E is bounded away from the inner boundary A, the continuity of the appropriate harmonic kernel[10] then forces $\max |\phi_j|$ to 0 as $j \to \infty$. To prove this, we assume the induction hypothesis. If g_j is the function harmonic on C satisfying Neumann condition N_j on A and Dirichlet condition 0 on B, then the jth inner solution is $\phi_j - g_j$, and the normal velocity jump is

$$T_j = \frac{\partial}{\partial n}\phi_j - \frac{\partial}{\partial n}(\phi_j - g_j) = \frac{\partial}{\partial n} g_j$$

on B. If $s(x)$ is the unit source, the source correction term is

$$\sigma_j(x) = \int_B T_j(\sigma) s(x - \sigma)\, dA(\sigma) \tag{B2}$$

here $\int_A \ldots$ or $\int_A \ldots dA(\sigma)$ refers to $n-1$ dimensional "area" integration on a hypersurface A in R^n, $\sigma \epsilon A$. By defining

$$\phi_{j+1} = \begin{cases} \phi_j - \sigma_j & \text{on } E \\ \phi_j - g_j - \sigma_j & \text{on } C \end{cases}$$

we find that there is no potential or normal velocity jump across B; thus the new ϕ_{j+1} can in fact be extended to A, and there it satisfies the Neumann condition

$$N_{j+1} = -\frac{\partial}{\partial n}\sigma_j$$

Therefore, to prove Eq. (B1), we need only show the following two inequalities (for some $c < 1$):

$$\int_B |T_j| = \int_B \left|\frac{\partial}{\partial n} g_j\right| \le \int_A |N_j| = \int_A \left|\frac{\partial}{\partial n} g_j\right| \tag{B3}$$

$$\int_A |N_{j+1}| = \int_A \left|\frac{\partial}{\partial n}\sigma_j\right| \le c \int_B |T_j| \tag{B4}$$

To prove Eq. (B3), suppose C is a finite region in R^n bounded by the disjoint union of hypersurfaces A and B, where B is closed. Furthermore, suppose ϕ is continuous in $\bar{C}$ (the closure of C), harmonic in C, and satisfies $\phi = 0$ on B. We claim that

$$\int_B \left|\frac{\partial \phi}{\partial n}\right| \le \int_A \left|\frac{\partial \phi}{\partial n}\right| \tag{B5}$$

Clearly one may assume $\partial\phi/\partial n$ integrable on A. Because of the existence of solutions to the L^1 Neumann/Dirichlet problem of this type, we may decompose a Neumann boundary condition on A into its positive and negative parts. Hence, it suffices to prove Eq. (B5) under the assumption $\partial\phi/\partial n \ge 0$ on A.

First we assume $\partial\phi/\partial n > 0$ on A. Suppose $\min_{A \cup B} \phi < 0$. By compactness this minimum must be attained at some point σ, which by the Dirichlet condition is in A. Since $\partial\phi(\sigma)/\partial n > 0$, there is a point σ' near σ and inside C such that $\phi(\sigma') < (\phi\sigma) = \min_{A \cup B} \phi$. This violates the minimum principle; hence our assumption implies $\phi \ge 0$ on $A \cup B$, and hence on $\bar{C}$. By a limiting argument involving harmonic kernel continuity, this implies that $\phi \ge 0$ on C, $\partial\phi/\partial n \le 0$ on B when $\partial\phi/\partial n \ge 0$ on A. By the divergence theorem,

$$\int_{A \cup B} \frac{\partial \phi}{\partial n} = \int_A \frac{\partial \phi}{\partial n} + \int_B \frac{\partial \phi}{\partial n} = 0$$

which implies Eq. (B5) and hence Eq. (B3).

Now, suppose U and V are connected open regions in R^n, U finite and convex, $\bar{U} \subset V$, with boundary hypersurfaces $A = \partial U$, $B = \partial V$. We claim that there exists $c < 1$ such that for any integrable function T on B, if we define $\sigma = \sigma_T$ on $R^n - B$ as in Eq. (B2), we get

$$\int_A \left|\frac{\partial \sigma}{\partial n}\right| \le c \int_B |T| \tag{B6}$$

For $\sigma \epsilon B$, define $\theta(\sigma, U)$ to be the solid angle subtended by U at σ. If we define θ_{TOT} to be the solid angle of the entire sphere in R^n, then by the convexity of U and a compactness argument $c = \sup_{\sigma \epsilon B} c(\sigma) < 1$, where

$$c(\sigma) = \frac{2\theta(\sigma, U)}{\theta_{\mathrm{TOT}}}$$

But a unit source at σ has as streamlines the radii from σ, and by spherical symmetry induces a total flux through U of $c(\sigma)/2$. By convexity, each streamline that meets U passes through A twice, hence

$$\int_A \left|\frac{\partial}{\partial n} s(x - \sigma)\right| dA(x) = c(\sigma) \le c \tag{B7}$$

Integration of Eq. (B7) yields Eq. (B6), which implies Eq. (B4). It is worth noting that the only place where the convexity of U is used is in getting the absolute integral of the flux through ∂U from a source on ∂V.

It is easy to see how the preceding arguments might be extended to a more general elliptic problem, with the source corrections being assumed small. (That assumption sometimes leads to under-relaxation in the method's application; see Sec. III.) In the present work we use the transonic small perturbation equation which has mixed character and is hyperbolic near A in this work. Heuristically, we may justify the application of the method by supposing an envelope A' which encloses the actual inner boundary and the hyperbolic region, and imagining that the inner boundary conditions are shifted to this elliptic envelope.

Acknowledgment

This work was supported partially by the Office of Naval Research, contract No. N00014-76-C-0931.

References

[1]Bauer, F., Garabedian, P., and Korn, D., "Theory of Supercritical Wing Sections," *Lecture Notes in Economics and Mathematical Systems,* Springer-Verlag, New York, 1972.

[2]Jameson, A., "Transonic Potential Flow Calculations using Conservation Form," *Proceedings, AIAA 2nd Computational Fluid Dynamics Conference,* 1975, pp. 148-161.

[3]Krupp, J.A. and Murman, E.M., "The Numerical Calculation of Steady Transonic Flows Past Thin Lifting Airfoils and Slender Bodies," AIAA Paper 71-566, Palo Alto, Calif., June 21-23, 1971.

[4]Klunker, E.B., "Contribution to Methods for Calculating the Flow About Thin Lifting Wings at Transonic Speeds-Analytic Expressions for the Far Field," NASA TN D-6530, 1971.

[5]Bailey, F.R. and Ballhaus, W.F., "Comparisons of Computed and Experimental Pressures for Transonic Flows about Isolated Wings and Wing-Fuselage Configurations," NASA SP-347, 1975, pp. 1213-1232.

[6]Schmidt, W., "Progress in Transonic Flow Computations," *Lecture Series 87,* von Karman Institute for Fluid Dynamics, March 15-19, 1976.

[7]Dickson, L.J., Chen, A.W., and Rubbert, P.E., "A New Approach to Far-Field Boundary Conditions in Transonic Computations," *Proceedings of the 5th International Conference on Numerical Methods in Fluid Dynamics,* Springer-Verlag, New York, 1976, pp. 173-178.

[8]Murman, E.M. and Cole, J.D., "Calculation of Plane Steady Transonic Flows," *AIAA Journal,* Vol. 9, Jan. 1971, pp. 114-121.

[9]Krupp, J.A., "The Numerical Calculation of Plane Steady Transonic Flows Past Thin Lifting Airfoils," Boeing Scientific Research Laboratories, Rept. D180-12958-1, 1971.

[10]Bergman, S. and Schiffer, M.M., *Kernel Functions and Elliptic Differential Equations of Mathematical Physics,* Academic Press, New York, 1953.